

Pattern Division Random Access (PDRA) for M2M Communications with Massive MIMO Systems

Xiaoming Dai, Tiantian Yan, Qianqian Li, Hua Li and Xiyuan Wang

Abstract

In this work, we introduce the pattern-domain pilot design paradigm based on a “*superposition of orthogonal-building-blocks*” with significantly larger contention space to enhance the massive machine-type communications (mMTC) random access (RA) performance in massive multiple-input multiple-output (MIMO) systems. Specifically, the pattern-domain pilot is constructed based on the superposition of L cyclically-shifted Zadoff-Chu (ZC) sequences. The pattern-domain pilots exhibit zero correlation values between non-colliding patterns from the same root and low correlation values between patterns from different roots. The increased contention space, i.e., from N to $\binom{N}{L}$, where $\binom{N}{L}$ denotes the number of all L -combinations of a set N , and low correlation values lead to a significantly lower pilot collision probability without compromising *excessively* on channel estimation performance for mMTC RA in massive MIMO systems. We present the framework and analysis of the RA success probability of the pattern-domain based scheme with massive MIMO systems. Numerical results demonstrate that the proposed pattern division random access (PDRA) scheme achieves an appreciable performance gain over the conventional one, while preserving the existing physical layer virtually unchanged. The extension of the “*superposition of orthogonal-building-blocks*” scheme to “*superposition of quasi-orthogonal-building-blocks*” is straightforward.

Index Terms—Pattern-domain, massive machine-type communications (mMTC), multiple-input multiple-output (MIMO), random access (RA), pattern division random access (PDRA).

Xiaoming Dai, Tiantian Yan, Qianqian Li, and Hua Li are with the School of Computer and Communication Engineering, University of Science and Technology Beijing, Beijing 100083, China (e-mail: daixiaoming@ustb.edu.cn).

Xiyuan Wang is with the School of Information and Communication Engineering, Beijing Information Science and Technology University, Beijing 100101, China (e-mail: wangxiyuan@bistu.edu.cn).

I. INTRODUCTION

The Internet of Things (IoT) is a novel paradigm to support connections of billions of miscellaneous innovative devices and will enable a range of new capabilities and services ranging from mission-critical services to massive deployment of autonomous devices [1]. As an enabler of the IoT, machine type communication [2] which involves a large number of user devices that communicate autonomously with the aim of forming a ubiquitous and automatic communication network without human intervention, has received tremendous interest among mobile network operators, equipment vendors, and research bodies. In a M2M scenario, a cellular base-station (BS) is required to connect to a large number of devices with typically sporadic activity patterns [2]. The sporadic traffic pattern may be due to the fact that devices are often designed to sleep most of the time in order to save energy and are activated only when triggered by external events, as is typically the case in a sensor network. Simultaneous random access attempts from massive sporadic machine-type communications (mMTC) devices may severely congest a shared physical random access channel (PRACH) in the current LTE and 5G networks [3] and cause intolerable delay, packet loss, and even service unavailability.

Various approaches have been proposed to improve the performance of LTE networks serving MTC devices. Leya *et al.* proposed to split the random access pilots into two sets to serve conventional data applications of user equipments (UEs) and short data applications of the mMTC devices separately [4].¹ With the group paging approach, Wei *et al.* introduced a model to estimate the number of successful and collided MTC devices in each random access slot [5]. Lee *et al.* proposed a group-based RA scheme, in which location-aware MTC devices located nearby are put into one group and tagged with the same group identifier [6]. Group-based access methods can accommodate a large number of MTC devices at the expense of prolonged access delay due to multi-hop transmissions. Slotted access proposed in [7] can mitigate congestion in light loads, however, it is not practical in massive connectivity load scenarios. The 3rd Generation Partnership Project (3GPP) introduced an access class barring (ACB) scheme [8] to reduce random access overload in cellular networks by broadcasting an ACB parameter ρ , where $0 \leq \rho \leq 1$, to all MTC devices via system information blocks (SIBs). The load is relieved by permitting base stations (BSs) to temporarily block low-priority devices, or reduce their probability of accessing the PRACH by a dynamic update of the relevant access parameters [9]. Reference [10] proposed

¹We utilize mMTC device and UE interchangeably throughout this work whenever there is no ambiguity.

a multi-preamble transmissions scheme with massive multiple-input multiple-output (MIMO) to mitigate the pilot collision at the cost of increased system resources and codeword ambiguity at receiver. Massive MIMO opens up new avenues for enabling highly efficient random access (RA) by offering an abundance of spatial degrees of freedom [11]–[13].

Despite the approaches [4]–[13] proposed from different angles, the size of pilots remains the limiting factor that determines the RA success probability. The conventional scheme dictates that the users contend for random access by uniformly choosing at random one pilot from a pre-specified pool of sequences [14]. In 3GPP LTE systems, the pilots are constructed from prime-length Zadoff-Chu (ZC) sequences with different cyclic shifts and root indexes [15].

Allocating more time/frequency physical resources for RA purposes can alleviate the pilot collision, however, it is obviously very costly in terms of spectral efficiency, which is of paramount importance in wireless system designs. In this paper, we introduce the pattern-domain pilot design paradigm based on a “*superposition of orthogonal-building-blocks*” to enlarge the size of contention space, without resorting to increasing physical resources. Specifically, a pattern-domain pilot is designed based on the superposition of K cyclically-shifted ZC sequences from a root index. The pattern-domain pilots are orthogonal between non-colliding patterns from the same root and exhibit low correlation values between patterns from different roots. For a cell with 32 cyclically-shifted ZC sequences and $L = 2$, the contention space is expanded by about $\binom{32}{2}/32 = \frac{32!}{32 \cdot 2! \cdot (32-2)!} \approx 16$ times. Since it is far less likely for multiple devices to choose an identical pattern, i.e., L cyclically-shifted ZC sequences, than it is to choose a single ZC sequence (i.e., $L = 1$ pattern), the pattern-domain based paradigm can significantly reduce the pilot collision probability without sacrificing *excessively* on channel estimation (this will be elucidated later in Section III-B and Section IV). As a result, the overall performance of the mMTC RA is enhanced.

We present the framework of analysis of the success probability of the proposed pattern division random access (PDRA) scheme in massive MIMO systems. Analysis illustrates that the proposed PDRA can reduce the pilot collision probability significantly without compromising excessively on the channel estimation and data detection performance. Simulation results demonstrate that the PDRA achieves an appreciable performance gain over the conventional one in massive MIMO systems, while keeping the existing physical layer virtually intact. We can extend the “superposition of orthogonal-building-blocks” to “superposition of *quasi*-orthogonal-building-blocks” in an straightforward manner.

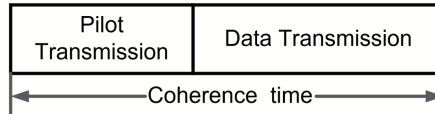


Fig. 1: Random access transmission structure.

The rest of this work is organized as follows: Section II describes the system model. The proposed PDRA scheme is detailed in Section III. Numerical results are provided in Section IV and are compared with the conventional scheme in Section IV. We conclude this work in Section V.

Notation: Vectors and matrices are denoted by boldface lowercase and uppercase letters, respectively. The transpose, complex conjugate, and conjugate transpose are represented by $(\cdot)^T$, $(\cdot)^*$, and $(\cdot)^H$, respectively. $\mathbf{r} \sim \mathcal{CN}(\mathbf{0}, \mathbf{R})$ indicates that \mathbf{r} is a circularly symmetric complex Gaussian (CSCG) random vector with zero-mean and covariance matrix \mathbf{R} . $\binom{m}{n} = \frac{m!}{n!(m-n)!}$ denotes the binomial coefficient. $\lfloor x \rfloor$ represents the greatest integer less than or equal to x . $X \sim \Gamma(\alpha, \beta)$ denotes that X is gamma-distributed with shape parameter α and scale parameter β . $\delta(\cdot)$ denotes the Dirac delta function.

II. SYSTEM MODEL

Consider a single-cell uplink M-MIMO system where the BS with $M (\gg 1)$ antennas serves single-antenna mMTC devices. The mMTC devices are assumed to be synchronized and each mMTC device decides in each coherence block whether or not to access the channel with probability ε in an independent and identically distributed (i.i.d.) manner [13]. On each RA occasion, we assume that there are N UEs active and contend with their uplink payloads by directly transmitting pilots with length N_{ZC} randomly selected from a pilot pool: $\mathcal{S} = \{\mathbf{s}_1, \mathbf{s}_2, \dots, \mathbf{s}_{N_p}\}$ followed by data transmission as illustrated in Fig. 1. The complex channel vector between the BS and the n -th mMTC device is given by $\mathbf{f}_n = \sqrt{\xi_n} \mathbf{h}_n \in \mathbb{C}^M$, where ξ_n denotes the large-scale fading value and $\mathbf{h}_n \sim \mathcal{CN}(0, \mathbf{I}_M)$ represents the small-scale fading coefficients. The channel is constant and frequency-flat for the transmission of pilot and data samples.

In commercial wireless systems, base stations transmit reference signals [14] that are used by the user equipment (UE) to estimate the pathloss [16]. The UE can then adjust its initial transmission power based on the measurement of the downlink reference signal power [16]. For

the sake of analytical traceability, we assume perfect power control of each active UE,² the received pilot $\mathbf{Y} \in \mathbb{C}^{M \times N_{\text{ZC}}}$ is expressed as:

$$\mathbf{Y} = \sum_{n=1}^N \sqrt{P} \mathbf{h}_n \mathbf{s}_n^T + \mathbf{W}, \quad (1)$$

where P denotes the expected received power for all UEs, and $\mathbf{W} \in \mathbb{C}^{M \times N_{\text{ZC}}}$ represents the noise matrix with each element distributed as $\mathcal{CN}(0, \sigma^2)$. The uplink signal-to-noise ratio (SNR) of each UE is defined as $\alpha_{\text{R}} \triangleq P/\sigma^2$.

The received data symbol vector $\mathbf{z} \in \mathbb{C}^M$ is given by:

$$\mathbf{z} = \sum_{n=1}^N \sqrt{P} \mathbf{h}_n d_n + \mathbf{n}, \quad (2)$$

where d_n represents the data symbol transmitted by the n -th UE and $\mathbb{E}[|d_n|^2] = 1$, \mathbf{n} denotes the background noise vector distributed as $\mathcal{CN}(0, \sigma^2 \mathbf{I}_M)$.

The BS is responsible for detecting the active devices, estimating their channels, and decoding the transmitted data based on the acquired channel estimates to accomplish coherent data transmission. If all the active UEs select different pilots, the BS can detect the set of active UEs, estimate their channels and decode data transmitted by the active UEs with adequate accuracy. Whereas, if multiple mMTC devices select the same pilot, the BS can not detect the collided user channels and the data detection will fail at the BS as a result of pilot collision. The number of antennas M is assumed to be sufficiently large in this work, so mutual orthogonality among the vector-valued channels to the UEs can be approximately achieved.

III. PATTERN DIVISION RANDOM ACCESS (PDRA) IN MASSIVE MIMO SYSTEMS

A. Proposed Pattern-domain Pilot Generation

In 3GPP 4G LTE and 5G NR systems, the pilots are generated from ZC sequences with different cyclic shifts and root indexes [15]. The set of pilots is first constructed from cyclic-shifts of a single root sequence, and then by cyclic shifts of different roots if necessary. A ZC sequence \mathbf{c}_u of odd length N_{ZC} derived from root u is defined as:

$$c_u[l] = e^{-j \frac{\pi u l(l+1)}{N_{\text{ZC}}}}, \quad 0 \leq l \leq N_{\text{ZC}} - 1, \quad (3)$$

²We abbreviate active UE as UE in later exposition if there is no ambiguity.

where the root u is relatively prime to N_{ZC} . The total number of roots is denoted by R .

The cyclic shift offset N_{CS} is dimensioned so that the zero correlation zone (ZCZ) of the sequences guarantees the orthogonality of the pilot sequences regardless of the delay spread and time uncertainty of the UEs. The N_{CS} enables unambiguous detection with timing uncertainty $\tau < N_{CS}$, which is given by:

$$N_{CS} \geq \left\lceil \left(\frac{2R_c}{c} + \tau_{\max} \right) \times N_{ZC} \times \Delta f_{RA} + n_g \right\rceil, \quad (4)$$

where R_c is the cell radius, $c \approx 3 \times 10^8$ is the speed of light, τ_{\max} is the maximum expected delay spread of the propagation channel, Δf_{RA} is the PRACH subcarrier spacing (SCS), and n_g are additional guard samples due to the pulse shaping filter. The size of the pilot subset constructed from a single root ZC sequence N_{SS} , i.e., sequence subset size is $N_{SS} = \lfloor \frac{N_{ZC}}{N_{CS}} \rfloor$.

ZC sequences derived from a single root ZC sequence are generated as:

$$c_{u,v}[l] = c_u[(l + C_v) \bmod N_{ZC}], \quad (5)$$

where $C_v = vN_{CS}$ with $0 \leq v \leq N_{SS} - 1$ represent the cyclic shifts. We denote ZC sequences derived from root u with cyclic shift v as: $\mathbf{c}_{u,v} = \{c_{u,v}[0], \dots, c_{u,v}[N_{ZC} - 1]\}$.

The periodic autocorrelation of the ZC sequence is zero for all off-peak shifts, and the cyclically-shifted ZC sequences constructed by a root sequences are orthogonal. The cross-correlation value between the ZC sequences constructed from different root sequences is $\sqrt{N_{ZC}}$ if N_{ZC} is a prime number.

Increasing the pilots allocated to the RA purpose can reduce the collision probability at the cost of resources for data transmission. Accounting for this, we expand the contention space to the pattern-domain in a single random access sub-frame without resorting to increasing the physical resources. In this paper, we introduce the pattern-domain pilot design scheme based on a ‘‘superposition of orthogonal-building-blocks’’ to enlarge the size of contention space. As an illustrative example, we propose to utilize the ZC sequence with prime length as the *building-block* to construct pattern with large pool size and desirable channel estimation property. Specifically, the pattern derived from root u is constructed based on the superposition of the L cyclically-shifted ZC sequences as follows:

$$\mathbf{s}_{u,i} = \frac{1}{\sqrt{L}} \underbrace{(\mathbf{c}_{u,v} + \mathbf{c}_{u,q} + \dots + \mathbf{c}_{u,s})}_{\text{Sum of } L \text{ terms}}, v \neq q \neq \dots \neq s \in \{0, \dots, N_{SS}-1\}, 0 < i < N_{PS} - 1, \quad (6)$$

where $N_{\text{PS}} = \binom{N_{\text{SS}}}{L}$ denotes the size of the pattern subset constructed from a single root, i.e., pattern subset size. The pilot pool \mathcal{S} designed based on the pattern-domain paradigm can be expressed as follows:

$$\mathcal{S} = \left\{ \mathbf{s}_{u_1,0} \cdots \mathbf{s}_{u_1,N_{\text{PS}}-1}, \mathbf{s}_{u_2,0} \cdots \mathbf{s}_{u_2,N_{\text{PS}}-1}, \mathbf{s}_{u_R,0} \cdots \mathbf{s}_{u_R,N_{\text{PS}}-1} \right\}, \quad (7)$$

where $N_{\text{P}} = RN_{\text{PS}}$ represents the pattern-domain pilot pool size. For the sake of illustration simplicity, we utilize \mathbf{s}_i to denote $\mathbf{s}_{u_r,i}$ with $u_r \in \{u_1, u_2, \dots, u_R\}$ in later exposition if there is no ambiguity. Based on (6) and (7), the pattern-domain pilots are orthogonal between non-colliding patterns derived from the same root and exhibit low correlation values between patterns derived from different roots.

The extension of the proposed ‘‘superposition of the orthogonal-building-blocks’’ to ‘‘superposition of the *quasi*-orthogonal-building-blocks’’ is straightforward. We may extend the superposition operation to more generic finite-field operations which can be left for future investigation. The developments in this work are first geared toward *insights* and then toward generality.

Compared to the conventional scheme, the pilot pool size of the proposed pattern-domain based paradigm is enlarged by:

$$\mu = \frac{R \binom{N_{\text{SS}}}{L}}{RN_{\text{SS}}} = \frac{\binom{N_{\text{SS}}}{L}}{N_{\text{SS}}}. \quad (8)$$

For the sake of simplicity, we only consider the pattern based on $L = 2$ cyclically-shifted ZC sequences in this work. For a typical cell configured with $N_{\text{SS}} = 32$, the size of the pilot pool N_{P} is enlarged by about 16 times without allocating more time/frequency physical resources.

Increasing the size of the pilot pool is not a complete solution to the problem of the RA success in a crowded cellular network since the RA performance depends not only on the probability of pilot collision but also on the probability of successful data detection. We elucidate the underlying idea of the proposed PDRA with massive MIMO systems in Section III-B.

B. Success Probability of PDRA in Massive MIMO Systems

For the sake of simplicity, the matched filter (MF) detector is applied at the BS to perform channel estimation and data detection. In order to successfully decode the data of an active UE, it is of paramount importance for the BS to acquire accurate channel state information (CSI) of active UEs in the case of no pattern collision and then performs data detection with adequate

accuracy to ensure active UEs exhibit sufficiently high signal-to-interference-and-noise-ratios (SINRs). The success probability of the RA depend on the following two factors:

- 1) Pattern collision: For a PDRA scheme, only if all ZC sequence components of an active UE collide with other UEs', the active UE will have no chance of recovering the data. In other words, the active UE can still obtain reasonably accurate CSI even with only one collision-free ZC sequence component.
- 2) Adequate SINR: Data transmission of an active UE is considered successful only when its SINR is sufficiently high.

Based on the aforementioned analysis, we define the probability of no pattern collision P_S and $P(\alpha_{\text{MF}} \geq \alpha_{\text{Th}})$ for the active UE as the success probability, where α_{MF} is the SINR of the active UE and α_{Th} is a given SINR threshold which depends on the modulation and coding schemes of the specific UE. (The subscript MF indicates that the matched filter is used as the detector at the base station.)

Without loss of generality, the success probability of the first UE P_{MF} is derived as follows:

$$P_{\text{MF}} = P_S P(\alpha_{\text{MF}}^1 \geq \alpha_{\text{Th}}) = P_S \sum_{K=0}^{N-1} P(K) \left[P_{E_0} P(\alpha_{\text{MF}}^1 \geq \alpha_{\text{Th}} | K, E_0) + P_{E_1} P(\alpha_{\text{MF}}^1 \geq \alpha_{\text{Th}} | K, E_1) \right], \quad (9)$$

- where P_S denotes the probability that no pattern collision occurs between the first UE and the other $N - 1$ UEs and is expressed as:

$$P_S = \left(1 - \frac{1}{RN_{\text{PS}}}\right)^{N-1} = \left(1 - \frac{1}{N_{\text{P}}}\right)^{N-1}, \quad (10)$$

- $P(K)$ denotes the probability that K other UEs choose the other $R - 1$ different root patterns from the first UE and the rest $N - 1 - K$ UEs select the same root patterns as the first active UE and is given by:

$$P(K) = \frac{\binom{N-1}{K} ((R-1)N_{\text{PS}})^K (N_{\text{PS}} - 1)^{N-1-K}}{(RN_{\text{PS}} - 1)^{N-1}}, \quad (11)$$

- E_0 denotes the event whereby the $N - 1 - K$ users have no single ZC sequence component colliding with the first UE and P_{E_0} represents the probability of the event E_0 occurring, which is expressed as:

$$P_{E_0} = \frac{((N_{\text{SS}} - 2)(N_{\text{SS}} - 3)/2)^{N-1-K}}{(N_{\text{PS}} - 1)^{N-1-K}}, \quad (12)$$

- $P(\alpha_{\text{MF}}^1 \geq \alpha_{\text{Th}} | K, E_0)$ represents the probability of $\alpha_{\text{MF}}^1 \geq \alpha_{\text{Th}}$ on the condition that K other UEs choose the other $R - 1$ different root patterns from the first active UE and the event E_0 occurs,
- E_1 denotes the event whereby the $N - 1 - K$ users have one single ZC sequence component colliding with the first UE and P_{E_1} represents the probability of the event E_1 occurring, which is given by:

$$P_{E_1} = \frac{2 \sum_{T=1}^{N-1-K} \binom{N-1-K}{T} (N_{\text{SS}} - 2)^T ((N_{\text{SS}} - 2)(N_{\text{SS}} - 3)/2)^{N-1-K-T}}{(N_{\text{PS}} - 1)^{N-1-K}}, \quad (13)$$

- $P(\alpha_{\text{MF}}^1 \geq \alpha_{\text{Th}} | K, E_1)$ represents the probability of $\alpha_{\text{MF}}^1 \geq \alpha_{\text{Th}}$ on the condition that K other UEs choose the other $R - 1$ different root patterns from the first active UE and the event E_1 occurs.

The detailed derivation of P_{E_0} and P_{E_1} is deferred to the Appendix Section.

For the sake of illustration clarity, we denote \mathbf{s}_k as the pattern used by UE k with a slight abuse of notation. Without loss of generality, we assume that the first UE utilizes pattern $\mathbf{s}_1 (= \frac{1}{\sqrt{2}}(\mathbf{c}_{1,1} + \mathbf{c}_{1,2}))$.

In the case of event E_0 occurring, multiplying \mathbf{Y} from the right-side by $\frac{\mathbf{s}_1^*}{\|\mathbf{s}_1\|}$, we obtain the estimated channel vector of the active UE1 as follows:

$$\begin{aligned} \mathbf{g}_{1,E_0} &= \mathbf{Y} \frac{\mathbf{s}_1^*}{\|\mathbf{s}_1\|} = \sqrt{P} \mathbf{h}_1 \mathbf{s}_1^T \frac{\mathbf{s}_1^*}{\|\mathbf{s}_1\|} + \underbrace{\sum_{k=2}^{K+1} \sqrt{P} \mathbf{h}_k \mathbf{s}_k^T \frac{\mathbf{s}_1^*}{\|\mathbf{s}_1\|}}_{K \text{ UEs with different roots}} + \underbrace{\sum_{m=K+2}^N \sqrt{P} \mathbf{h}_m \mathbf{s}_m^T \frac{\mathbf{s}_1^*}{\|\mathbf{s}_1\|}}_{N-1-K \text{ UEs with the same root}} + \mathbf{W} \frac{\mathbf{s}_1^*}{\|\mathbf{s}_1\|} \\ &= \sqrt{P} \mathbf{h}_1 \mathbf{s}_1^T \frac{\mathbf{s}_1^*}{\|\mathbf{s}_1\|} + \underbrace{\sum_{k=2}^{K+1} \sqrt{P} \mathbf{h}_k \mathbf{s}_k^T \frac{\mathbf{s}_1^*}{\|\mathbf{s}_1\|}}_{K \text{ UEs with different roots}} + \mathbf{W} \frac{\mathbf{s}_1^*}{\|\mathbf{s}_1\|} = \sqrt{PN_{\text{ZC}}} \mathbf{h}_1 + \sum_{k=2}^{K+1} 2 \sqrt{P} \mathbf{h}_k + \tilde{\mathbf{w}}, \end{aligned} \quad (14)$$

where $\tilde{\mathbf{w}} = \mathbf{W} \frac{\mathbf{s}_1^*}{\|\mathbf{s}_1\|} \sim \mathcal{CN}(\mathbf{0}, \sigma^2 \mathbf{I}_M)$.

With the MF receiver, the estimate of the data symbol of the first UE is given by:

$$d_1 = \mathbf{g}_{1,E_0}^H \mathbf{z} = \sqrt{P} \mathbf{g}_{1,E_0}^H \mathbf{h}_1 d_1 + \sum_{n=2}^N \sqrt{P} \mathbf{g}_{1,E_0}^H \mathbf{h}_n d_n + \mathbf{g}_{1,E_0}^H \mathbf{n}. \quad (15)$$

Utilizing (15), we obtain the SINR of the first UE α_{MF}^1 as:

$$\alpha_{\text{MF}}^1 = \frac{P |\mathbf{g}_{1,E_0}^H \mathbf{h}_1|^2}{\sum_{n=2}^N P |\mathbf{g}_{1,E_0}^H \mathbf{h}_n|^2 + \|\mathbf{g}_{1,E_0}^H\|^2 \sigma^2} \stackrel{M \rightarrow \infty}{=} \frac{N_{\text{ZC}}}{4K}. \quad (16)$$

Equation (16) is derived based on the fact $\frac{\mathbf{h}_n^H \mathbf{h}_n}{M} \xrightarrow{M \rightarrow \infty} 1$ and $\frac{\mathbf{h}_n^H \mathbf{h}_k}{M} \xrightarrow{M \rightarrow \infty} 0$ when $n \neq k$. The detailed derivation of α_{MF}^1 is deferred to the Appendix Section. Based on (16), the asymptotic value of $P(\alpha_{\text{MF}}^1 \geq \alpha_{\text{Th}} | K, E_0)$ can be expressed as

$$\lim_{M \rightarrow \infty} P(\alpha_{\text{MF}}^1 \geq \alpha_{\text{Th}} | K, E_0) = 1_{K \leq \frac{N_{\text{ZC}}}{4\alpha_{\text{Th}}}} = \begin{cases} 1, & \text{if } K \leq \frac{N_{\text{ZC}}}{4\alpha_{\text{Th}}}, \\ 0, & \text{otherwise.} \end{cases} \quad (17)$$

In the case of event E_1 occurring, multiplying \mathbf{Y} from the right-side by $\frac{\mathbf{c}_{1,1}^*}{\|\mathbf{c}_{1,1}\|}$, we obtain the channel vector of the first UE as follows:

$$\begin{aligned} \mathbf{g}_{1,E_1} &= \mathbf{Y} \frac{\mathbf{c}_{1,1}^*}{\|\mathbf{c}_{1,1}\|} = \sqrt{\frac{P}{2}} \mathbf{h}_1 (\mathbf{c}_{1,1} + \mathbf{c}_{1,2})^T \frac{\mathbf{c}_{1,1}^*}{\|\mathbf{c}_{1,1}\|} + \underbrace{\sum_{k=2}^{K+1} \sqrt{\frac{P}{2}} \mathbf{h}_k (\mathbf{c}_{k,1} + \mathbf{c}_{k,2})^T \frac{\mathbf{c}_{1,1}^*}{\|\mathbf{c}_{1,1}\|}}_{K \text{ UEs with different roots}} \\ &+ \underbrace{\sum_{m=K+2}^N \sqrt{\frac{P}{2}} \mathbf{h}_m (\mathbf{c}_{m,1} + \mathbf{c}_{m,2})^T \frac{\mathbf{c}_{1,1}^*}{\|\mathbf{c}_{1,1}\|}}_{N-1-K \text{ UEs with the same root}} + \mathbf{W} \frac{\mathbf{c}_{1,1}^*}{\|\mathbf{c}_{1,1}\|} \\ &= \sqrt{P \frac{N_{\text{ZC}}}{2}} \mathbf{h}_1 + \sum_{k=2}^{K+1} 2 \sqrt{\frac{P}{2}} \mathbf{h}_k + \bar{\mathbf{w}}, \end{aligned} \quad (18)$$

where $\bar{\mathbf{w}} = \mathbf{W} \frac{\mathbf{c}_{1,1}^*}{\|\mathbf{c}_{1,1}\|} \sim \mathcal{CN}(\mathbf{0}, \sigma^2 \mathbf{I}_M)$. Similar to that of (16), we can obtain the same SINR value for the event E_1 .

Substituting (10)–(13), (16) and (17) into (9), we obtain the success probability of the P_{MF} as follows:

$$\begin{aligned} P_{\text{MF}} &= P_S \sum_{K=0}^{N-1} P(K) \left[P_{E_0} P\left(\frac{N_{\text{ZC}}}{4K} \geq \alpha_{\text{Th}}\right) + P_{E_1} P\left(\frac{N_{\text{ZC}}}{4K} \geq \alpha_{\text{Th}}\right) \right] = P_S \sum_{K=0}^{N-1} \left[P(K) (P_{E_0} + P_{E_1}) P\left(\frac{N_{\text{ZC}}}{4K} \geq \alpha_{\text{Th}}\right) \right] \\ &= P_S \sum_{K=0}^{N-1} \left[P(K) (P_{E_0} + P_{E_1}) 1_{K \leq \frac{N_{\text{ZC}}}{4\alpha_{\text{Th}}}} \right] = P_S \sum_{K=0}^{\min\left\{\left\lfloor \frac{N_{\text{ZC}}}{4\alpha_{\text{Th}}}\right\rfloor, N-1\right\}} P(K) (P_{E_0} + P_{E_1}) \\ &= \left(1 - \frac{1}{N_P}\right)^{N-1} \sum_{K=0}^{\min\left\{\left\lfloor \frac{N_{\text{ZC}}}{4\alpha_{\text{Th}}}\right\rfloor, N-1\right\}} \frac{\binom{N-1}{K} ((R-1)N_{\text{PS}})^K (N_{\text{PS}}-1)^{N-1-K}}{(RN_{\text{PS}}-1)^{N-1}} \\ &\times \left(\frac{((N_{\text{SS}}-2)(N_{\text{SS}}-3)/2)^{N-1-K}}{(N_{\text{PS}}-1)^{N-1-K}} + \frac{2 \sum_{T=1}^{N-1-K} \binom{N-1-K}{T} (N_{\text{SS}}-2)^T ((N_{\text{SS}}-2)(N_{\text{SS}}-3)/2)^{N-1-K-T}}{(N_{\text{PS}}-1)^{N-1-K}} \right). \end{aligned} \quad (19)$$

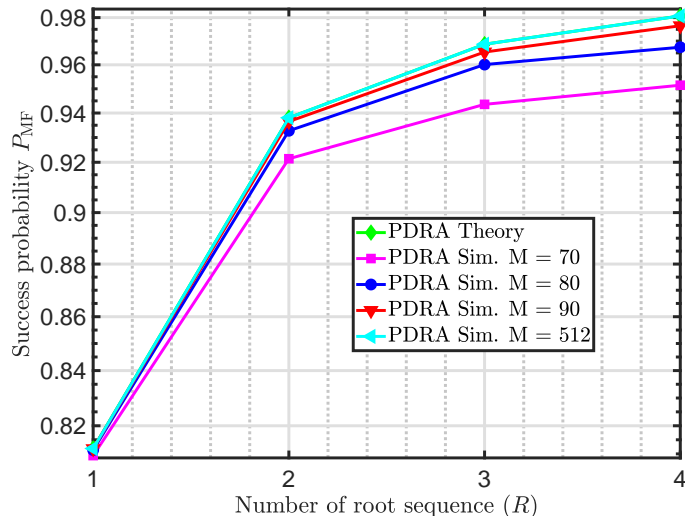


Fig. 2: P_{MF} as a function of R with different values of M , when $N_{SS} = 32$, $N = 10$, and $\alpha_{Th} = 5$ dB.

We will verify the accuracy of the asymptotic analysis of (19) in Section IV and study its behaviour for a finite (but large) M .

IV. NUMERICAL RESULTS

In this section, numerical results are first carried out to verify the asymptotic analysis of the PDRA in Section III-B. We then carry out system simulation of the success probability PDRA and compare it with the conventional one with various parameters.

A. Asymptotic Analysis of PDRA

Numerical results are first carried out to verify the asymptotic analysis of the PDRA in Section III-B. Fig. 2 illustrates the success probabilities as a function of R with different values of M when $N_{SS} = 32$, $N = 10$, and $\alpha_{Th} = 5$ dB. Fig. 2 shows that the numerical results (abbreviated as Sim.) closely match the analysis of (19) (labelled as Theory) of P_{MF} in Section III-B for large M and tighter results are observed as M grows. The result of $M = 512$ antennas is almost indistinguishable from that of the theoretical analysis [c.f. (19)]. As expected, the gap between the numerical and analytical results slightly increases as the M decreases since the mutual orthogonality among the vector-valued channels are not fully satisfied in that case.

B. System Simulations Parameters

In this section, we show numerically how the proposed PDRA performs in cellular networks. We consider the scenario which is composed of 19 hexagonal grid shaped cells, distributed in

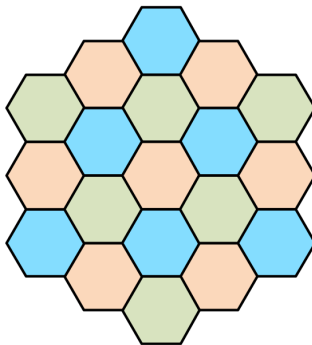


Fig. 3: Illustration of the cell topology.

three different tiers as depicted in Fig. 3. Two different channel models are considered in the simulations. The first one is uncorrelated Rayleigh fading, where $\mathbf{f}_n \sim \mathcal{CN}(0, \mathbf{I}_M)$. The second one is the spatially correlated Rayleigh fading channel with $\mathbf{f}_n \sim \mathcal{CN}(\mathbf{0}, \xi_n \mathbf{R}_n)$, where we consider a uniform linear array (ULA) at the BS modeled by the exponential correlation model with the correlation coefficient ρ between adjacent antennas $[\mathbf{R}_n]_{i,j} = \rho^{-|j-i|} e^{j\delta_n(j-i)}$, where δ_n is the angle between BS and active UE n . This represents a non-line-of-sight (NLoS) scenario with spatial correlation, indicating that the channel is statistically stronger in some spatial directions (determined by δ_n) than other directions. The pathloss is modeled based on the urban micro scenario [17]. The Rayleigh fading cases have a pathloss exponent of 3.8 and shadow fading with log-normal distribution and a standard deviation of 10 dB, while the line-of-sight (LoS) case has a pathloss exponent of 2.5 and log-normal variations with a standard deviation of 4 dB. The radius of each hexagon is 500 m, and the UEs are uniformly distributed in the cell at locations further than 30 m from the BS. We consider a scenario with 10,000 inactive UEs in the cell, where each UE accesses the network with probability P_A in a given RA opportunity. The signal-to-noise-ratio (SNR) is defined as the expected pattern to noise power ratio at each antenna port of the BS. The pattern length N_{ZC} is set to be 839 as the existing RA in 4G LTE and 5G NR standards [15].

1) *Success Probability Under Uncorrelated Rayleigh Fading Channel:* Fig. 4 illustrates the success probabilities as a function of R with different values of N_{SS} . As the N_{SS} increases, the success probability of both schemes improves and the proposed PDRA achieves an appreciable performance gain over the conventional one as illustrated in Fig. 4. It is also shown in Fig. 4 that the PDRA with $N_{SS} = 32$ even slightly outperforms the conventional one with $N_{SS} = 64$ for

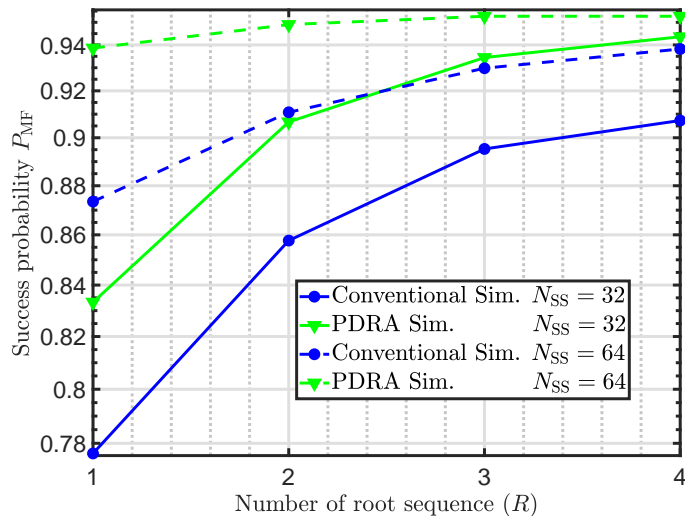


Fig. 4: P_{MF} as a function of root number R with different values of N_{SS} , when $M = 128$, $\alpha_{Th} = 5$ dB and $P_A = 0.1\%$.

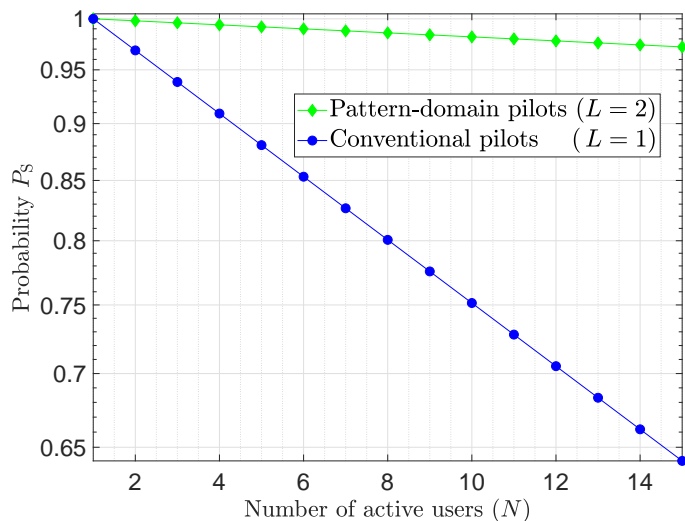


Fig. 5: P_S as a function of of active users with different values of L , when $N_{SS} = 32$.

$R > 2$.

This can be explained as follows: The success probability of P_{MF} is determined by two factors: 1) P_S ; and 2) $P(\alpha_{MF}^1 \geq \alpha_{Th})$. Increasing the number of pilots can alleviate the pattern collision P_S as shown in Fig. 5, however, the associated non-orthogonality also degrades the channel estimation and data detection performance [c.f. (16)]. Nonetheless, the performance gain derived from the collision probability reduction (due to the increase of contention space) outweighs the degradation of channel estimation and data detection caused by the non-orthogonality of the

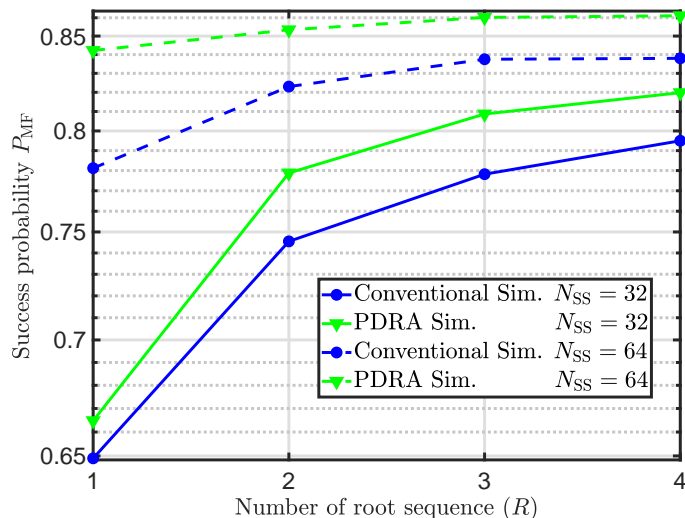


Fig. 6: P_{MF} as a function of root number R with different values of N_{SS} , when $M = 128$, $\alpha_{Th} = 5$ dB and $P_A = 0.15\%$.

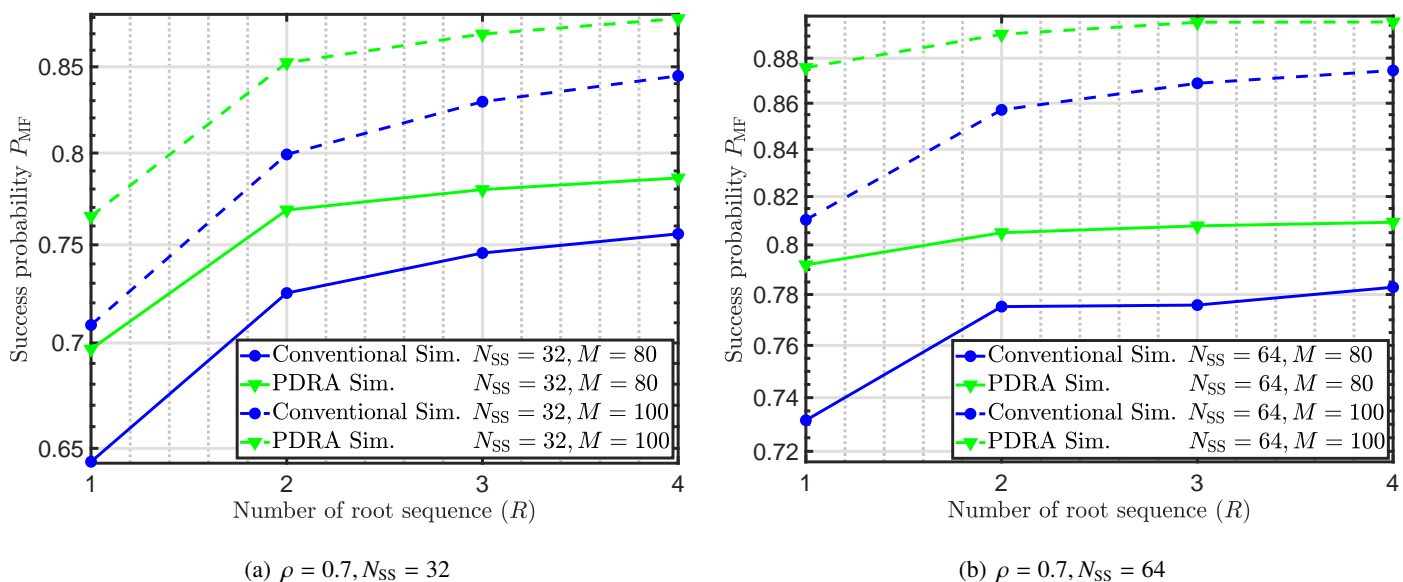


Fig. 7: P_{MF} as a function of root number R with different values of N_{SS} and M under the spatially correlated Rayleigh fading channel, when $\rho = 0.7$, $\alpha_{Th} = 5$ dB and $P_A = 0.1\%$.

patterns.

A similar phenomenon can be observed for a higher user activity probability P_A as illustrated in Fig. 6.

2) *Success Probability Under A More Realistic Channel Model:* We consider a ULA at the BS modeled with the correlation $\rho = 0.7$ between adjacent antennas. As expected, the success

probability of both schemes degrade under the spatially correlated Rayleigh fading channel due to the channel spatial correlations among antennas as shown in Figs. 7(a) and 7(b) [c.f. Fig. 4]. The performance degradation is lessened for BS with more antennas since the effect of channel spatial correlations can be mitigated in that case. Figs. 7(a) and 7(b) also illustrate that the proposed PDRA achieves similar performance gains over the conventional one as those of the uncorrelated channel models in Fig. 4.

Remark 1: For the sake of analytical tractability, we utilize the MF as the channel estimation and data detection method in this work. It is anticipated that greater performance gain can be realized via more advanced channel estimation and data detection methods, such as the linear minimum-mean-squared-error (LMMSE) based approach. The purpose of this work is to shed new light on potential directions of the pilot design for RA in massive MIMO systems, rather than on the not-so-prominent-performance-gain of the PDRA with the simple *MF* receiver. The developments in this work are first geared toward insights and then toward generality. We hope that the pattern-domain based approach may provide further impetus for innovative pilot designs for massive connectivity.

V. CONCLUSION

We introduce the pattern-domain pilot design paradigm based on a “superposition of the orthogonal-building-blocks” for mMTC device random access in massive MIMO systems in this work. The proposed pattern-domain pilots have a much larger pool size than that currently used in the 4G LTE and 5G NR standards and include the latter as a subset. Analysis is carried out to give insights into the performance gain of the PDRA over the conventional one. Numerical results demonstrate that the PDRA with the MF receiver can reduce pilot collision probability significantly without compromising *excessively* on channel estimation and data detection performance. The performance of the PDRA can be further enhanced via more advanced channel estimation and data detection methods (rather than the simple MF receiver).

We can extend the pattern-domain pilot design to more generic “superposition of the quasi-orthogonal-building-blocks” and/or finite-field operation based scheme which can be left for future investigation.

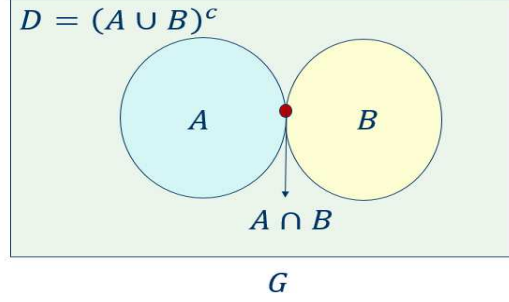


Fig. 8: The groups of pilots chosen by the users.

APPENDIX A

DERIVATION OF P_{E_0} AND P_{E_1}

For the sake of illustration clarity, we utilize Q to represent the number of distinct ZC sequences in the pilot pool, c_i to denote the i -th ZC sequence, and M to represent the number of UEs. Consider the situation that there are M UEs and each UE selects two different ZC sequences from the pilot pool. It is worth noting that the selection of c_1c_2 is considered to be the same as c_2c_1 . The UE1 is assumed to have selected pilots c_1c_2 . We divide the pilots selected by the other users into the following groups:

- 1) The entire space is defined as universal set $G = \{c_n c_m | 1 \leq n, m \leq Q, n \neq m\}$, and the number of elements of G is expressed as $g = (a + 1)(a + 2)/2$, where $a = Q - 2$.
- 2) The set of pilots with c_1 and excluding c_2 is defined as $A = \{c_1 c_n | 3 \leq n \leq Q\}$, and the number of elements of A is equal to a .
- 3) The set of pilots with c_2 and excluding c_1 is defined as $B = \{c_2 c_n | 3 \leq n \leq Q\}$, and the number of elements of B is equal to a .
- 4) The set of pilots excluding c_1 and c_2 is defined as a complement set of the union of A and B , $D = (A \cup B)^c = \{c_n c_m | 3 \leq n, m \leq Q, n \neq m\}$, and the number of elements of this set is expressed as $d = a(a - 1)/2$.
- 5) $A \cap B$ is a singleton containing only one element $c_1 c_2$, that is $A \cap B = \{c_1 c_2\}$.

The illustration of sets A, B, D , and G is depicted in Fig. 8.

P_{E_1} is defined as probability of the event that there is only one pilot collision for UE1, i.e., either c_1 or c_2 collides with other UEs, which is expressed as

$$P_{E_1} = 2 \frac{\binom{M-1}{0} d^0 a^{M-1} + \binom{M-1}{1} d a^{M-2} + \dots + \binom{M-1}{M-2} d^{M-2} a}{g^{(M-1)}} = 2g^{-(M-1)} \sum_{i=0}^{M-2} \binom{M-1}{i} d^i a^{M-1-i}. \quad (20)$$

P_{E_0} is defined as probability of the event that there is no pilot collision for UE1, i.e., neither c_1 nor c_2 collide with other UEs, which is given by:

$$P_{E_0} = \left(\frac{d}{g}\right)^{M-1}. \quad (21)$$

APPENDIX B

DERIVATION OF α_{MF}^1

We first unfold $\mathbf{g}_{1,E_0}^H \mathbf{h}_1$ and $\mathbf{g}_{1,E_0}^H \mathbf{h}_n$ as follows:

$$\mathbf{g}_{1,E_0}^H \mathbf{h}_1 = \sqrt{PN_{ZC}} \mathbf{h}_1^H \mathbf{h}_1 + \sum_{k=2}^{K+1} 2\sqrt{P} \mathbf{h}_k^H \mathbf{h}_1 + \tilde{\mathbf{w}}^H \mathbf{h}_1, \quad (22)$$

$$\mathbf{g}_{1,E_0}^H \mathbf{h}_n = \sqrt{PN_{ZC}} \mathbf{h}_1^H \mathbf{h}_n + \sum_{k=2}^{K+1} 2\sqrt{P} \mathbf{h}_k^H \mathbf{h}_n + \tilde{\mathbf{w}}^H \mathbf{h}_n. \quad (23)$$

For the sake of convenience, we rewrite (16) of the manuscript as follows:

$$\begin{aligned} \alpha_{MF}^1 &= \frac{P |\mathbf{g}_{1,E_0}^H \mathbf{h}_1|^2}{\sum_{n=2}^N P |\mathbf{g}_{1,E_0}^H \mathbf{h}_n|^2 + \|\mathbf{g}_{1,E_0}^H\|^2 \sigma^2} \\ &\stackrel{(a)}{\approx} \frac{P \left(PN_{ZC} M + \sum_{k=2}^{K+1} 4P + \sigma^2 \right)}{P \sum_{n=2}^N \left(PN_{ZC} + \sum_{k=2, k \neq n}^{K+1} 4P + \sum_{k=2}^{K+1} 4PM \delta(k-n) + \sigma^2 \right) + \left(PN_{ZC} + \sum_{k=2}^{K+1} 4P + \sigma^2 \right) \sigma^2} \\ &\stackrel{(b)}{=} \frac{\alpha_R^2 N_{ZC} M + 4\alpha_R^2 K + \alpha_R}{\alpha_R^2 (N-1) N_{ZC} + 4\alpha_R^2 (K(N-1) - K) + 4\alpha_R^2 KM + \alpha_R (N-1) + \alpha_R N_{ZC} + 4\alpha_R K + 1} \\ &\stackrel{(c)}{\approx} \frac{\alpha_R^2 N_{ZC} M}{4\alpha_R^2 KM} \\ &= \frac{N_{ZC}}{4K}. \end{aligned} \quad (24)$$

(a) follows from the fact that 1) $\frac{|\mathbf{h}_n^H \mathbf{h}_n|^2}{M} \xrightarrow{M \rightarrow \infty} M$ and $\frac{|\mathbf{h}_n^H \mathbf{h}_n|}{M} \xrightarrow{M \rightarrow \infty} 1$; 2) Utilizing (22) and (23), we obtain $\frac{P |\mathbf{g}_{1,E_0}^H \mathbf{h}_1|^2}{M} \xrightarrow{M \rightarrow \infty} P^2 N_{ZC} \frac{|\mathbf{h}_1^H \mathbf{h}_1|^2}{M} + \sum_{k=2}^{K+1} 4P^2 \frac{|\mathbf{h}_k^H \mathbf{h}_1|^2}{M} + \frac{P \sigma^2 \|\mathbf{h}_1\|^2}{M}$, $\frac{\sigma^2 \|\mathbf{g}_{1,E_0}^H\|^2}{M} = \frac{\sigma^2 \|\sqrt{PN_{ZC}} \mathbf{h}_1^H + \sum_{k=2}^{K+1} 2\sqrt{P} \mathbf{h}_k^H + \tilde{\mathbf{w}}^H\|^2}{M}$ and $\frac{P |\mathbf{g}_{1,E_0}^H \mathbf{h}_n|^2}{M} \xrightarrow{M \rightarrow \infty} P^2 N_{ZC} \frac{|\mathbf{h}_1^H \mathbf{h}_n|^2}{M} + \sum_{k=2}^{K+1} 4P^2 \frac{|\mathbf{h}_k^H \mathbf{h}_n|^2}{M} + \frac{P \sigma^2 \|\mathbf{h}_n\|^2}{M}$; 3) As $M \rightarrow \infty$, $\frac{|\mathbf{h}_k^H \mathbf{h}_n|}{M}$ obeys the Gamma distribution $\Gamma(1, 1)$ when $k \neq n$.

(b) is derived based on $\alpha_R = P/\sigma^2$.

(c) follows from the fact that the non- M part of the denominator of the third line of (24) is negligible compared with those of the M -part, as $M \rightarrow \infty$.

REFERENCES

- [1] “More than 50 billion connected devices,” Stockholm, Sweden, Ericsson, White Paper, 2011.
- [2] R. Q. Hu, Y. Qian, H. Chen and A. Jamalipour, “Recent progress in Machine-to-Machine communications,” *IEEE Commun. Mag.*, vol. 49, no. 4, pp. 24–26, Apr. 2011.
- [3] Z. Wang and Vincent W. S. Wong, “Optimal access class barring for stationary machine type communication devices with timing advance information,” *IEEE Trans. Wireless Commun.*, vol. 14, no. 10, pp. 5374–5387, Oct. 2015.
- [4] A. Laya, L. Alonso, and J. Alonso-Zarate, “Is the random access channel of LTE and LTE-A suitable for M2M communications? A survey of alternatives,” *IEEE Commun. Surveys Tuts.*, vol. 16, no. 1, pp. 4–16, first Quart. 2014.
- [5] C. Wei, R. Cheng and S. Tsao, “Modeling and estimation of one-shot random access for finite-user multichannel slotted ALOHA systems,” *IEEE Communi. Lett.*, vol. 16, no. 8, pp. 1196–1199, Aug. 2012.
- [6] K. Lee *et al.*, “A group-based communication scheme based on the location information of MTC devices in cellular networks,” in *Proc. IEEE Int. Conf. Commun. (ICC)*, Ottawa, ON, Canada, Jun. 2012, pp. 4899–4903.
- [7] 3GPP R2–103759 (2010). Load distribution for MTC devices, ALU/ASB, RAN270-bis.
- [8] “Study on RAN improvements for machine-type communications,” 3GPP, Sophia Antipolis, France, Tech. Rep. 37.868 V14.0.0, Sep. 2017.
- [9] T.-M. Lin, C.-H. Lee, J.-P. Cheng, and W.-T. Chen, “PRADA: Prioritized random access with dynamic access barring for MTC in 3GPP LTE-A networks,” *IEEE Trans. Veh. Technol.*, vol. 63, no. 5, pp. 2467–472, Jun. 2014.
- [10] S. Vural, N. Wang, G. Foster and R. Tafazolli, “Success probability of multiple-preamble-based single-attempt random access to mobile networks,” in *IEEE Communi. Letters*, vol. 21, no. 8, pp. 1755–1758, Aug. 2017.
- [11] J. Ding, D. Qu, H. Jiang and T. Jiang, “Success probability of grant-free random access with massive MIMO,” *IEEE Internet of Things Journal*, vol. 6, no. 1, pp. 506–516, Feb. 2019.
- [12] L. Liu and W. Yu, “Massive connectivity with massive MIMO Part I: Device activity detection and channel estimation,” *IEEE Trans. Signal Process.*, vol. 66, no. 11, pp. 2933–2946, Jun. 2018.
- [13] K. Senel and E. G. Larsson, “Grant-free massive MTC-enabled massive MIMO: a compressive sensing approach,” *IEEE Trans. Communi.*, vol. 66, no. 12, pp. 6164–6175, Dec. 2018.
- [14] Evolved Universal Terrestrial Radio Access (E-UTRA) ; Medium Access Control (MAC) Protocol Specification; Release 13, 3GPP TS 36. 321, 2017.
- [15] S. Sesia, M. Baker, and I. Toufik, *LTE-the UMTS Long Term Evolution: from Theory to Practice*. John Wiley & Sons, 2011.
- [16] Technical Specification Group Radio Access Network, NR, Physical Layer Procedures, TS 36.213 V15.0.0, Dec. 2017.
- [17] “Spatial Channel Model for Multiple Input Multiple Output (MIMO) Simulations (Release 13) ”, document TR 25. 996, 3GPP, Dec. 2019.